Late Quaternary Glaciations on the Chukchi Margin, Arctic Ocean: Insights from Echo Sounding and Sediment Records

Y. J. Joe[1], L. Polyak[2], K. Jang[1, 3], C. Vogt[4], S. Kim[5], J.-H. Kim[1], Y. K. Jin[1], J. K. Hong[1], F. Niessen[6], and S.-I. Nam[1]

[1]Division of Glacier and Earth Sciences, Korea Polar Research Institute, 21990, Incheon, Republic of Korea.

[2]Byrd Polar and Climate Research Center, The Ohio State University, 1090 Carmack Road, Columbus, OH, 43210, USA.

[3]Department of Earth System Sciences, Yonsei University, 03722, Seoul, Republic Korea.

[4]Crystallography & Geomaterials Research (GEO 2360) Faculty of Geosciences at the University of Bremen, 28359, Germany.

[5]Ocean Climate Response & Ecosystem Research Department, Korea Institute of Ocean Science & Technology, 49111, Busan, Republic of Korea.

[6]Alfred Wegener Institute (AWI) Helmholtz Centre for Polar and Marine Research, D-27568, Bremerhaven, Germany.

Corresponding author: Seung-Il Nam (sinam@kopri.re.kr)

Key Points:

- The core-seismic integration provides stratigraphic constraints for the glacigenic submarine bedforms on the Chukchi Rise.
- Spatial variability in sediment composition among the studied cores represents glaciation centers on the Chukchi and East Siberian margins.
- The penultimate East Siberian Ice Sheet had an especially strong impact on seafloor erosion and deposition into the western Arctic Ocean.

Abstract

Glacigenic bedforms such as multiple glacial lineations and moraines on the Chukchi and East Siberian margins reveal recurrent waxing and waning by voluminous ice masses. Despite their paleoclimatic significance, the timing, geographic distribution, and mechanisms of these glaciations remain inadequately understood. To enhance our understanding of the Quaternary Arctic glacial history, we study high-resolution swath bathymetry and subbottom profiling data with lithostratigraphy and provenance of four sediment cores. These data characterize deposits of the last two glaciations at the Chukchi margin and adjacent basins. In all cores, multiple peaks of plagioclase are prominent in both glacial intervals, probably reflecting predominant glacigenic input from the East Siberian Ice Sheet (ESIS). Peaks of dolomite and quartz for tracing the Laurentide Ice Sheet sources occur around the last glacial/deglacial interval and in sediment preceding the penultimate glaciation. By integrating seismostratigraphy with sediment cores, we constrain the formation of mid-slope moraines on the western side of the Chukchi Rise to the penultimate glaciation (estimated age range MIS 4 to 6). Considering the coeval glacial erosion off the East Siberian margin, our results confirm that the ESIS at that time extended to water depths of ~650/950 m on the Chukchi Rise/East Siberian margin. In comparison, the last ESIS (MIS 2 to possibly 4) was smaller, with the identified seafloor imprint limited to water depths of ~450 m on the Chukchi Borderland, while its extent on the East Siberian margin remains to be determined.

1 Introduction

The Arctic ice sheets, which were partially marine-based, played an important role in the Earth's climate system throughout the Quaternary glacial-interglacial cycles [*Hu et al.*, 2010; *Peltier*, 2007]. The growth and retreat of ice sheets at the Arctic perimeter resulted in reshaping seafloor on the adjacent shelves and borderlands [*Jakobsson et al.*, 2014 and references therein; *S Kim et al.*, 2021; *O'Regan et al.*, 2017] along with shifts in sediment inputs and ocean circulation in the Arctic Ocean [*Clark et al.*, 1980; *Dong et al.*, 2020; *Jakobsson et al.*, 2016; *Jang et al.*, 2013; *Stein et al.*, 2010; *Xiao et al.*, 2021]. In this context, the Arctic Ocean sedimentary records provide valuable geological evidence for reconstructing the glacial history and related oceanographic changes.

Investigations of the impact of Quaternary glaciations on the Arctic Ocean have been focused mainly on the large continental Eurasian and Laurentide ice sheets (EAIS, LIS) [*Dalton et al.*, 2019; *Dalton et al.*, 2022; *Gasson et al.*, 2018; *Stein et al.*, 2010; *Svendsen et al.*, 2004]. However, seismostratigraphic and swath bathymetry records from the Chukchi/East Siberian margin provide increasing evidence for the past presence of a mostly marine-based East Siberian ice sheet (ESIS) (Fig. 1a) [*Dove et al.*, 2014; *Jakobsson et al.*, 2008; *S Kim et al.*, 2021; *Niessen et al.*, 2013]. The repeated occurrence of this voluminous ice sheet occupying a large portion of the East Siberian and Chukchi shelves constitutes a previously overlooked, important component of the Arctic glacial system. Recently collected geophysical and sediment core records suggest that the major ESIS expansion into the Arctic Ocean eroded the Arliss Plateau off the East Siberian margin (Fig. 1b) at water depths of ~950 m (mwd) during the late Quaternary [*Joe et al.*, 2020; *Schreck et al.*, 2018]. A set of glacigenic bedforms, including contour-parallel recessional moraines on the Chukchi Rise, an extension of the Chukchi margin (Fig. 1b), were probably coeval with the glacial erosion on the Arliss Plateau [*S Kim et al.*, 2021]. Furthermore, geological fingerprints of the younger glaciation have been found in multiple sediment cores

from the East Siberian/Chukchi margin and the adjacent Chukchi basin [*Joe et al.*, 2020; *Schreck et al.*, 2018; *Rujian Wang et al.*, 2013; *Xiao et al.*, 2024; *Ye et al.*, 2020]. Despite these advances, the timing, geographic distribution, and mechanisms of these glacial events are poorly understood.

In this study, we investigate high-resolution swath bathymetry and subbottom profiling data and sediment cores from the Chukchi Rise and the adjacent Chukchi and Northwind basins (Fig. 1b). Our goal is to develop an integrated regional seismo- and lithostratigraphy and to identify depositional processes and sediment sources from the glaciated areas. Results will provide new insights into the Late Pleistocene glacial history at the perimeter of the western Arctic Ocean.2 Materials and Methods

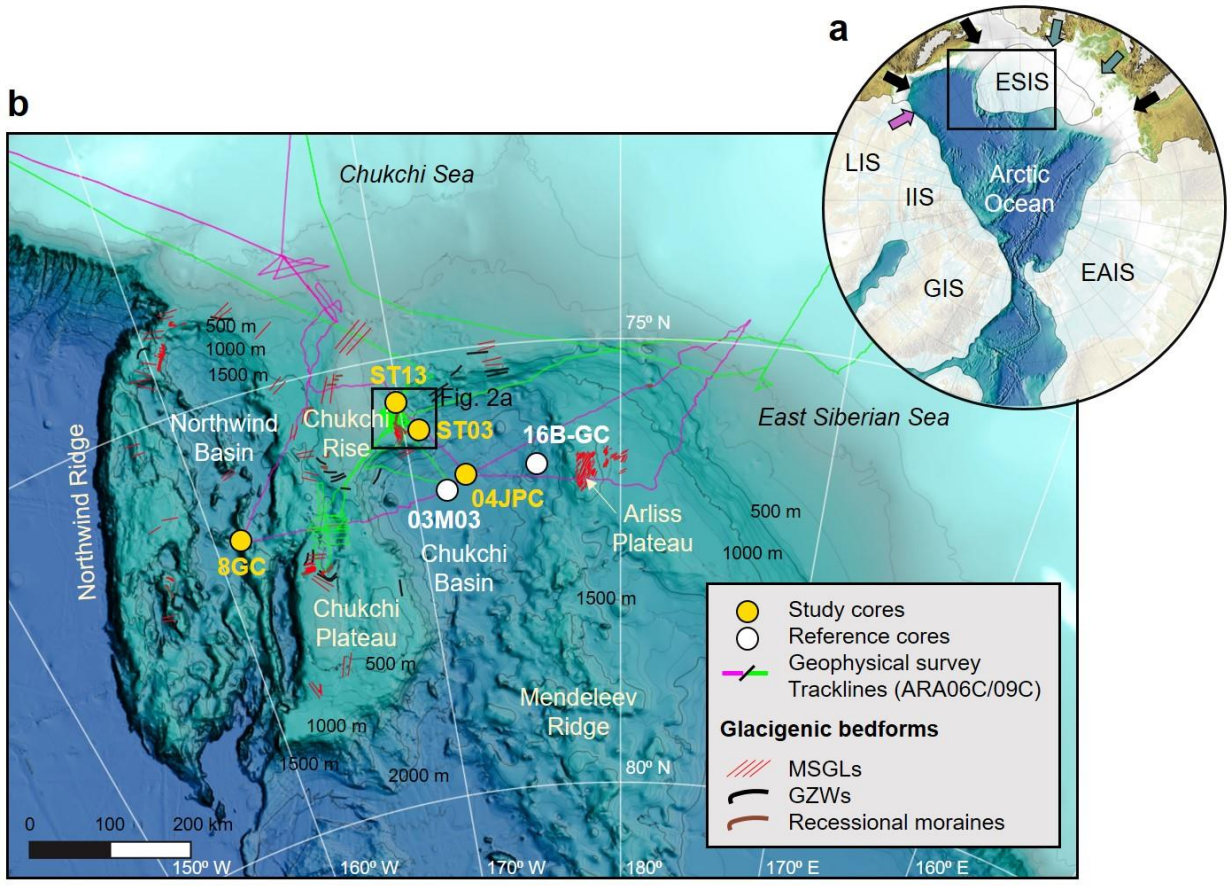

Figure 1. Physiographic maps of the Arctic Ocean (a) and study area (b) from IBCAO v4 [*Jakobsson et al.*, 2020]. In Fig. 1a, ice-sheet outlines from *Batchelor et al.* [2019]. GIS, LIS, IIS, EAIS, and ESIS - Greenland, Laurentide, Innuitian, Eurasian, and East Siberian ice sheets. Black, purple, and green arrows indicate inputs of quartz, detrital carbonate including dolomite, and plagioclase from source regions, respectively. Fig. 1b presents sediment cores, survey track lines, and glacigenic bedforms. Yellow and white circles show cores from this study and references, respectively. For regional distributions of glacigenic bedforms, we used a shapefile from *Streuff et al.* [2021]. MSGL and GZWs – mega-scale glacial lineations and grounding zone wedges.

2 Regional background

2.1 Sedimentation in the western Arctic Ocean

The Arctic Ocean is surrounded by the Eurasian and North American land masses, which comprise complex terrains and associated lithologies [*Fagel et al.*, 2014]. The peripheral geology of Eurasia and North America has been used to infer the sediment provenances in the Arctic Ocean [e.g., *Dong et al.*, 2017; *Phillips and Grantz*, 2001; *Zhang et al.*, 2021]. The Arctic marine sediments are Quartz-dominant, which reflect variable quartz-bearing bedrock geologies of the Arctic peripheries. [*Phillips and Grantz*, 2001]. These ubiquitous provenances of quartz hamper determining their origins in the western Arctic Ocean. However, feldspar is relatively abundant in the East Siberian and Laptev seas compared to quartz [*Darby et al.*, 2011; *Vogt*, 1997]. In this regard, the quartz/feldspar ratio (Q/F) in the western Arctic Ocean presents a decreasing trend from the North American margin (>2.5) to the East Siberian margin (<1.0), hence utilizing as an effective index to distinguish the origin of the quartz source [*Darby et al.*, 2011; *Kobayashi et al.*, 2016; *Yamamoto et al.*, 2017; *Zhao et al.*, 2022; *Zou*, 2016]. In the East Siberian and western Chukchi seas, marine sediments present increases in igneous rock fragments and plagioclase [*Zhang et al.*, 2021; *Zou*, 2016]. Their distribution possibly indicates that coastal erosion and river runoff from the northeast Siberian continent, including the Okhotsk-Chukotka volcanic belt, contributes sediment input to the East Siberian and Chukchi margins (Fig. 1) [*Dong et al.*, 2017; *Viscosi-Shirley et al.*, 2003; *Zhang et al.*, 2021]. Detrital carbonates, including dolomite, are common in the western Arctic Ocean compared to the eastern Arctic Ocean [*Phillips and Grantz*, 2001]. Radiogenic isotope studies indicate that the Paleozoic carbonate platform in CAA is the main source of detrital carbonates in the western Arctic Ocean [*Bazhenova et al.*, 2017; *Dong et al.*, 2020; *Fagel et al.*, 2014]. In particular, the deposition of detrital carbonates is mainly identified as pinkish coarse sediment layers in the Holocene and earlier sediment records from the western Arctic Ocean, which indicates the collapse events of the Laurentide Ice Sheet in Northern America (Fig. 1) [*Dong et al.*, 2017; *Jang et al.*, 2013; *Phillips and Grantz*, 2001; *Stein et al.*, 2010; *Rujian Wang et al.*, 2013; *Xiao et al.*, 2020].

2.2 Glacigenic submarine landforms and seismostratigraphy

Distinct, multiple glacigenic submarine landforms (bedforms) have been observed on the seafloor of the East Siberian/Chukchi margin and the adjacent borderland (Fig. 1b). These features include mega-scale glacial lineations (MSGLs), morainic ridges, grounding zone wedges (GZWs), subglacial till deposits, as well as pervasive iceberg scours [*Dove et al.*, 2014; *Jakobsson et al.*, 2008; *S Kim et al.*, 2021; *Niessen et al.*, 2013; *O'Regan et al.*, 2017; *Polyak et al.*, 2007; *Polyak et al.*, 2001]. On the Chukchi side, the deepest MSGL fields are found at depths exceeding 900 mwd. At shallower depths (600-700 mwd), contour-parallel, nested recessional moraines, and grounding zone wedges characterize the seafloor of the Chukchi Rise and Plateau. The shallowest bedform clusters are found at ~350-460 mwd of the Chukchi Rise and the southern Northwind Ridge, comprising MSGLs and subglacial till deposits [*Dove et al.*, 2014; *S Kim et al.*, 2021]. On the East Siberian side, several sets of MSGLs are identified between 900 and 1,200 mwd, including the MSGL set on top of the Arliss Plateau at 950 mwd [*Niessen et al.*, 2013]. The shallowest glacigenic feature is identified on the East Siberian slope at ~650-700 mwd [*Niessen et al.*, 2013].

Seismic reflection and acoustic investigations reveal that glacigenic sedimentary units truncate pre-glacial strata on the outer shelf and upper slope of the Chukchi/East Siberian margin [*Dove et al.*, 2014; *Jakobsson et al.*, 2008; *S Kim et al.*, 2021; *Lehmann and Jokat*, 2022; *Lehmann et al.*, 2022; *Niessen et al.*, 2013]. Stacked debris lobes on the middle to lower slopes indicate voluminous sediment transport towards the adjacent basins, associated with the advance and retreat of marine-based ice sheets [*Dove et al.*, 2014; *Joe et al.*, 2020; *S Kim et al.*, 2021]. The deep basins off the Chukchi and East Siberian shelves act as depocenters for sediments originating from ice-sheet margins and associated debris flows.

3 Materials and Methods

3.1 Data collection

3.1.1 Geophysical survey data

Multi-beam echo sounding (MBES) and high-resolution CHIRP subbottom profiling (SBP) data were collected on the western Chukchi Rise during several expeditions of the RV *Araon* in 2012-2019 (ARA03B-ARA10C) [*S Kim et al.*, 2021]. In this study, we use the MBES data recorded in a setting with a wide beam angle (-65° to 65°) and ARA09C SBP data with a frequency range of 2.5-7.0 kHz. Mapped swath bathymetry with a 20-m grid resolution was superimposed on the International Bathymetric Chart of the Arctic Ocean [IBCAO v. 4; *Jakobsson et al.*, 2020].

3.1.2 Sediment cores

This study uses four sediment cores from the Chukchi Rise and adjacent Chukchi and Northwind basins (Fig. 1b and Table 1). Two gravity sediment cores, ARA09C/ST13-GC and ARA09C/ST03-GC (hereafter ST13 and ST03), from the western flank of the Chukchi Rise, were taken in front of a recessional moraine and from a sediment drape on the MSGL field, respectively (Fig. 2B). ARA06C/04JPC (hereafter 04JPC) was taken with a jumbo piston corer near a previously studied core 03M03 from the Chukchi Basin [*Rujian Wang et al.*, 2013]. ARA03B/08GC (hereafter 8GC) was obtained from the Northwind Basin, which was reported by *Schreck et al.* [2018]. In this study, only the upper parts of two cores, 04JPC and 8GC, are presented for stratigraphic comparison with the Chukchi Rise cores (ST13 and ST03).

Table 1. Information on studied and reference cores.

Cruise	Station	Long. (E°)	Lat. (N°)	Water depth (m)	References
ARA06C	04JPC	-172.68	76.43	2292	This study
ARA09C	ST03	-170.32	75.92	829	This study Koo et al. (2021)
ARA09C	ST13	-169.74	75.67	624	This study Koo et al. (2022)
ARA03B	8GC	-160.78	76.60	2160	This study Schreck et al. (2018)
ARA02B	16B-GC	-175.97	76.40	1841	Joe et al. (2020)
ARC2	M03	-171.93	76.54	2300	Wang et al. (2013)

3.2 Sediment core analyses

3.2.1 Surface image, sediment color, and X-ray fluorescence (XRF) measurements

To provide a general characterization of lithostratigraphy, we employed core surface images, sediment color indices L* (black-white) and a* (green-red), and X-ray fluorescence (XRF) elemental composition. For two Chukchi Rise cores, ST13 and ST03, sediment color indices were measured with a Minolta CM 2500d spectrophotometer on board during the *Araon* expedition in 2018 (ARA09C). Surface images and elemental compositions of these cores were obtained using an ITRAX scanner at the Korea Polar Research Institute (KOPRI). The ITRAX scanner was equipped with a molybdenum (Mo) X-ray source operating at 30 kV and 30 mA with a measurement time of 10 seconds. For the other two cores (04JPC and 8GC), sediment color indices, surface images, and elemental compositions were measured with the Avaatech XRF core scanner at the Korea Institute of Geoscience and Mineral Resources (KIGAM) [see *Schreck et al.*, 2018, for detailed measurement settings]. Manganese (Mn) and calcium (Ca) contents defined major lithostratigraphic markers, such as Mn-enriched brown layers and detrital carbonate interlayers. The down-core content of Mn was normalized to iron (Fe) to eliminate the potential dilution effect of background sedimentation [*Ferrat et al.*, 2012]. Normalization did not include aluminum (Al) due to the possibility of unstable measurements when using a Mo X-ray source. To determine the deposition of detrital carbonates, Ca values were normalized to strontium (Sr) [*Hodell et al.*, 2008].

3.2.2 Grain size analysis

To analyze grain size, this study used approximately 130 mg of freeze-dried bulk sediment. Sediment samples were treated with 35% for 24 hours to decompose the organic matter and then rinsed with deionized water. Each sample was sonicated with an ultrasonic vibrator before the analysis. For cores ST13, ST03, and 8GC, the grain size was measured with a Malvern Mastersizer 3000 Laser Diffraction Particle Size Analyzer at KOPRI. The grain size analysis of core 04JPC was conducted using a Mastersizer 2000 at KIGAM.

3.2.3 X-ray diffraction (XRD) measurement

The bulk mineral composition of core sediments was measured by X-ray diffraction (XRD) analysis. For two cores, 04JPC and 8GC, the XRD analysis was conducted using a Philips X'Pert Pro diffractometer equipped with a Cu-tube and Monochromator at the Crystallography & Geomaterials Research Faculty of Geosciences of the University of Bremen, Germany. Before the analysis, dried bulk sediment samples were ground to a fine powder (particle size <20 μm) and prepared using the Philips backloading system. Detailed measurement settings are described in *Vogt* [2009]. Quantitative determination of Mineral contents was conducted using the QUAX full-pattern analysis software [cf. *Vogt et al.*, 2002]. For other cores (ST13 and ST03), the bulk mineral composition was taken from earlier published data [*H-J Koo et al.*, 2021; *H J Koo et al.*, 2022].

3.2.4 AMS ^{14}C age dating

For ^{14}C dating, we used carbonate tests of planktic foraminifers, mainly *Neogloboquadrina pachyderma* (sin.), from two cores, ST03 and 04JPC (Table 2). Accelerator mass spectrometry ^{14}C analysis was performed at the MICADAS laboratory of the Alfred-

Wegener Institute, Germany. For ^{14}C age calibration, we used the Calib 8.20 program (http://calib.org) with the Marine 20 dataset [*Heaton et al.*, 2020]. Calendar years were calculated by applying marine reservoir ages of 800 and 1400 years as carbonate reservoir correction for Holocene and pre-LGM Arctic Ocean sediments, respectively [*Coulthard et al.*, 2010; *Hanslik et al.*, 2010].

Table 2. AMS ^{14}C ages and calibrated ages for planktic species *N. pachyderma* in two cores 04JPC and ST03 by Calibration program CALIB 8.20 and Marine20 dataset.

Lab ID	Core	Depth (cm)	^{14}C age (yr BP)	Reservoir (yr)	Calib age median probability (ka BP)
AWI 4253.1.1	ARA06C/04JPC	5-6	7,835±94	800	7.3
AWI 4254.1.1	ARA06C/04JPC	113-114	31,294±568	1400	33.5
AWI 12110.1.1	ARA09C/ST03	151-152	>37,723	1400	>40.4
AWI 12111.1.1	ARA09C/ST03	159-160	>37,723	1400	
AWI 12112.1.1	ARA09C/ST03	166-167	>37,723	1400	
AWI 12113.1.1	ARA09C/ST03	181-182	>37,723	1400	
AWI 12114.1.1	ARA09C/ST03	186-187	>37,723	1400	

4 Results

4.1 Echo sounding records

4.1.1 Acoustic characteristics

The western flank of the Chukchi rise can be divided into three sectors based on the seafloor geometry (Fig. 2): 1) the inner sector with high relief (~10-30 m high), 2) the depressed middle sector with a smooth geometry, and 3) the outer sector with low relief (~5-10 m high) (Fig. 2b). In the inner sector, the subseafloor records are characterized by well-stratified sediments among the acoustically transparent materials (Fig. 2c). An acoustically transparent material at ~620 mwd is wedge-shaped with an erosive basal contact, which coincides with the outermost part of contour-parallel recessional moraines (Fig. 2a) [*S Kim et al.*, 2021]. The outermost moraine is up to 45 m thick, and its distal flank is covered by stratified sediments (Figs. 2c, 3a). Downslope from the moraine, at least six acoustically (semi)transparent materials with 10-30 m highs are observed without distinct lower boundary (Fig. 2c). There is also no identifiable acoustic stratification even at their top. These bathymetric highs are identified as mound-type morphologies [Fig. 2 in *Y-G Kim et al.*, 2020]. Beyond the mound area, subseafloor records present overall well-stratified reflection throughout the middle to outer sectors. The well-stratified sedimentary succession thins outward. Despite the thinning of the sedimentary succession, the internal reflection patterns remain well, which allows us to trace reflectors with variable acoustic amplitudes from the middle sector to the outer sector. The outer sector with low relief corresponds to a field of SSW-NNE trending MSGLs (Fig. 2A) [*S Kim et al.*, 2021].

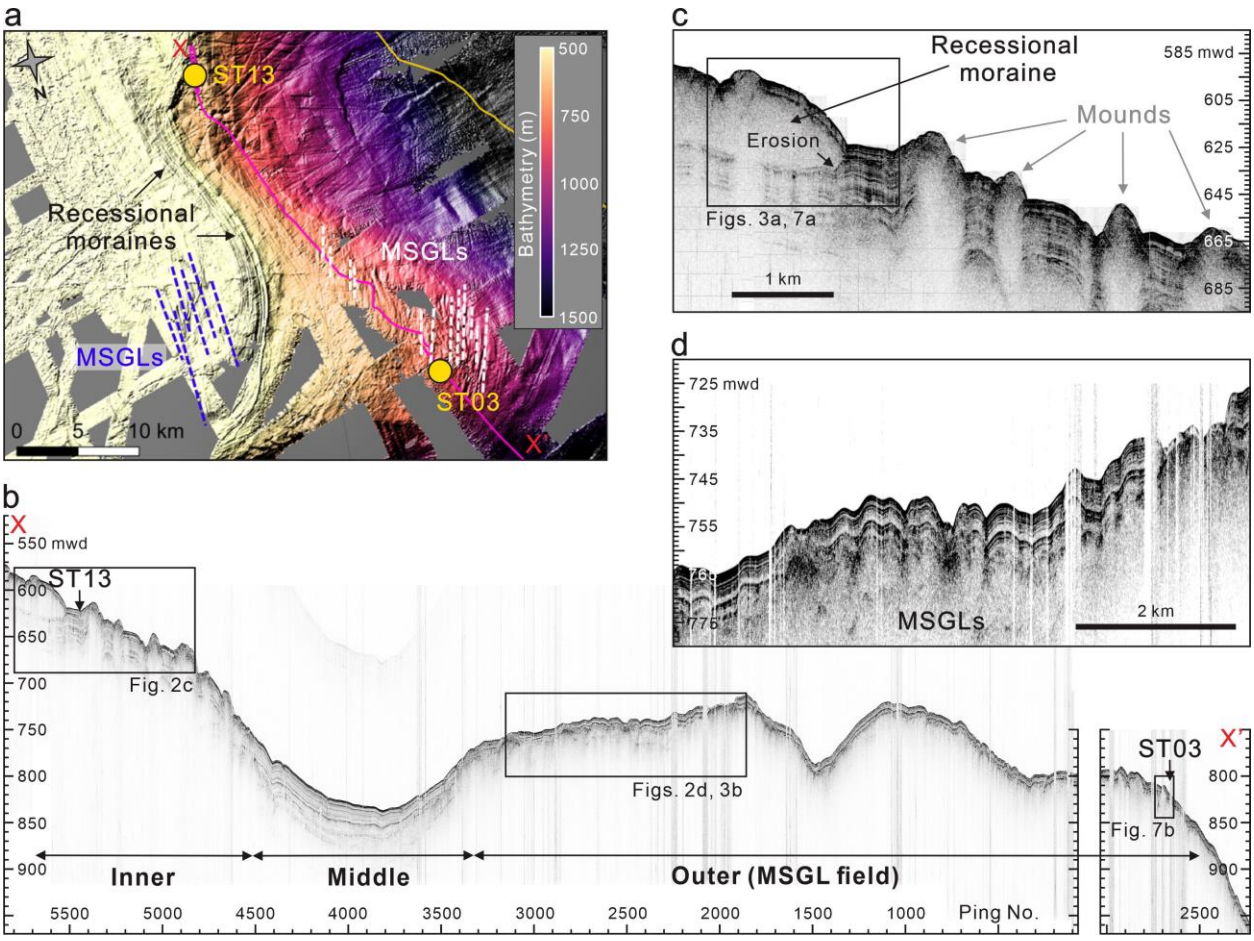

Figure 2. (a) Multibeam bathymetry and (b-d) subbottom profiling data from the western Chukchi Rise. See Fig. 1 for area location. MSGL - megascale glacial lineations.

4.1.2 Seismostratigraphy

In the well-stratified sedimentary succession, three prominent reflectors (R1, R2, and R_m) can be defined on the basis of their strong reflectivity, lateral continuity, and stratigraphic position with the recessional moraine (Figs. 3a, b). R1 represents the seafloor surface. A laterally continuous, strong reflector between R1 and the top of the recessional moraine is defined as R2. R_m is closely related to the erosive lower boundary of the recessional moraine (Fig. 3a). The acoustically (semi)transparent mounds downslope from the recessional moraine hinder tracking reflectors. However, the three defined reflectors on the MSGL field could be determined based on consistent reflection patterns in the stratified succession beyond the mound area. As a result, the top of the buried MSGLs lies stratigraphically below R_m (Fig. 3b). R1 and R2 correspond to the high-amplitude seismic reflections H1 and H2 defined by *S Kim et al.* [2021], respectively. R_m has the same stratigraphic position with a lower boundary of unit T2, interpreted as a grounding zone wedge and/or glacigenic debris flow deposits on the Chukchi Rise and its western slope in *S Kim et al.* [2021].

A sedimentary layer bounded by R1 and R2 is designed as a seismostratigraphic unit 1 (SSU 1). The SSU 1 consists of parallel, laterally continuous reflectors with moderate to strong amplitudes. Near the outermost recessional moraine, this unit is about 3 m thick and thins to

about 1.5 m on the MSGL field (Figs. 3a, b). Below SSU 1, SSU 2, which is bounded by R2 and R_m, can be further divided into two subunits by a reflector indicating the top of the moraine (Fig. 3a). Near the moraine, the upper subunit is characterized by subparallel, discontinuous reflectors with weak to moderate amplitudes. The lower subunit, related to the moraine formation, presents somewhat chaotic echo characters. In particular, this subunit has an unconformable contact with the slightly folded older sediments. On the MSGL field, SSU 2 is characterized by laterally continuous reflectors with moderate to strong amplitudes parallel to the geometry of the MSGL top (Fig. 3b). This reflection pattern blurs downward, becoming more transparent. SSU 2 is about 3.5-4 m thick in front of the moraine and thins to about 3 m on the MSGL field.

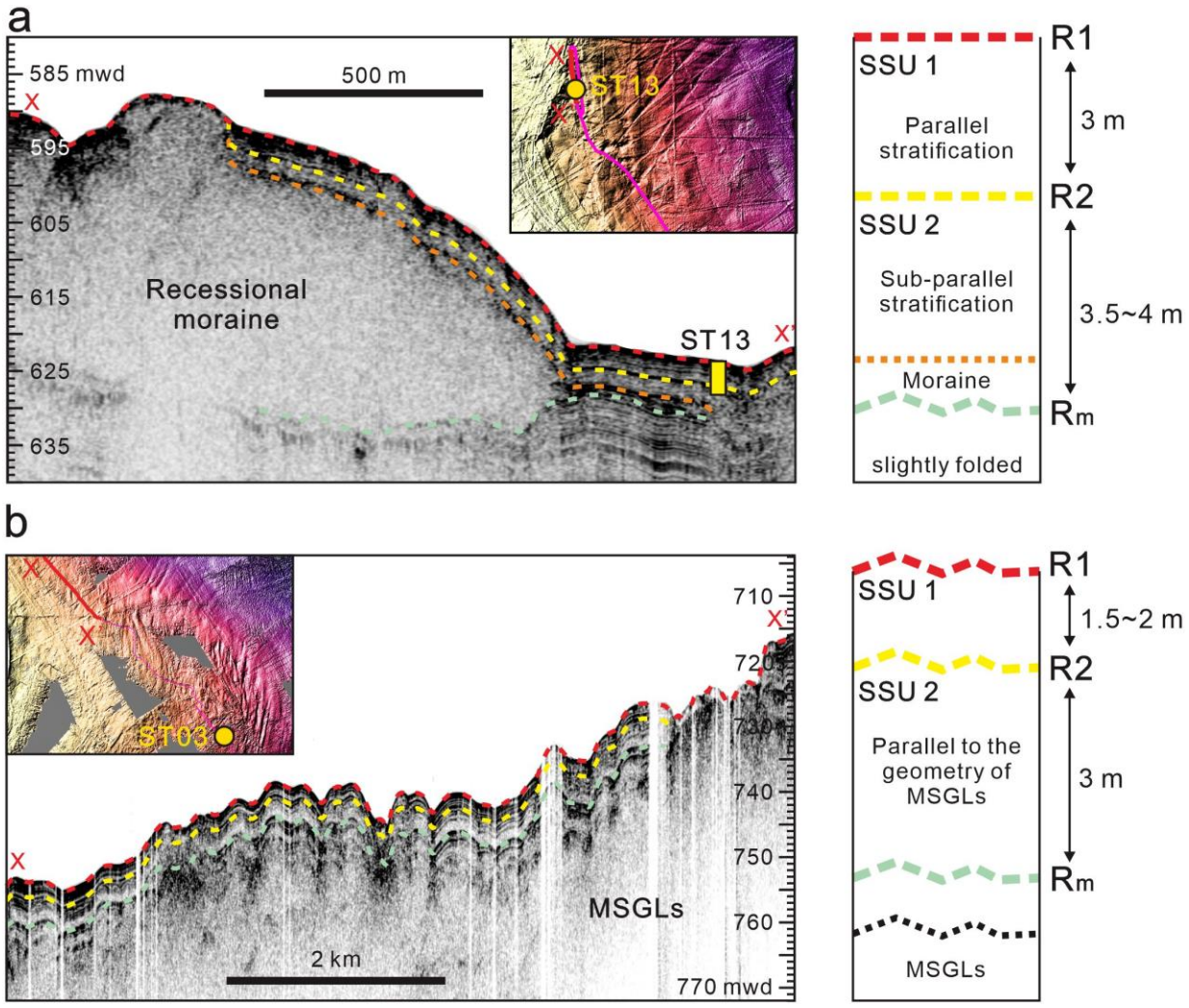

Figure 3. Zoom in on subbottom profiles characterized by glacigenic bedforms on the western Chukchi Rise with a seismostratigraphic explanation. (a) Recessional moraine on the western slope of Chukchi Rise. (b) Buried MSGLs on the lower slope.

4.2 Sediment core records

4.2.1 Lithostratigraphy

Four sediment cores from the Chukchi Rise and adjacent Chukchi and Northwind basins are mainly characterized by alternations of brownish and grayish layers, similar to many Arctic Ocean sediment records [e.g., *Jakobsson et al.*, 2000; *Polyak et al.*, 2009; *Stein et al.*, 2010] (Fig. 4). In addition, the transition zones between the brown and gray layers may be composed of yellowish and/or olive sediments. Several peaks of Mn content (expressed as Mn/Fe ratio) are observed in each core (Fig. 4). The increase in Mn content is matched with relatively low L* (darker) and high a* (reddish) values. Most brown, Mn-enriched layers have a relatively sharp and even upper boundary and a bioturbated lower boundary with brown mottles (red box in Fig. 4). In this study, these explicitly Mn-enriched intervals are defined as the B units (B1-4) (Fig. 4). Some of the transitional intervals, such as at 240-280 cm in core 8GC (blue box in Fig. 4), have interlaminated high- and low-Mn layers, apparently without bioturbation. Similar interlamination has been reported for other cores off the Chukchi/East Siberian margin [*Rujian Wang et al.*, 2013; *Xiao et al.*, 2024].

Grayish units (G) are more variable in color and are overall thicker than the brown units (Fig. 4). The upper gray unit (G1) between B1 and B2 generally thins out from the Chukchi Rise (cores ST13 and ST03) toward the basins. However, the second gray unit (G2) between B2 and B3 is thicker in the Chukchi Basin (core 04JPC) than on the Chukchi Rise. The Mn content of grayish units is overall low. In cores 8GC, ST13, and ST03 from the Northwind Ridge and Chukchi Rise, the upper part of G1 consists of dark gray sediment containing pinkish particles with an increase in Ca expressed as the Ca/Sr ratio (Fig. 4). This gray interval is massive at its bottom but becomes more stratified toward the top with alternating lighter and darker layers. In this study, we define this interval as a dark gray (DG) unit. Below this unit, a prominent Ca peak is identified above B2 in all cores. This interval generally consists of pinkish-white sediments with relatively high L* and a* values. Another pinkish layer with an abrupt increase in Ca content is observed near B3. The stratigraphic positions of these two intervals are consistent with the peaks of pinkish-white detrital carbonates in cores from the western Arctic Ocean, where the upper peak has been designated as W3 [*Clark et al.*, 1980; *Jang et al.*, 2023; *Polyak et al.*, 2009; *Schreck et al.*, 2018; *Stein et al.*, 2010].

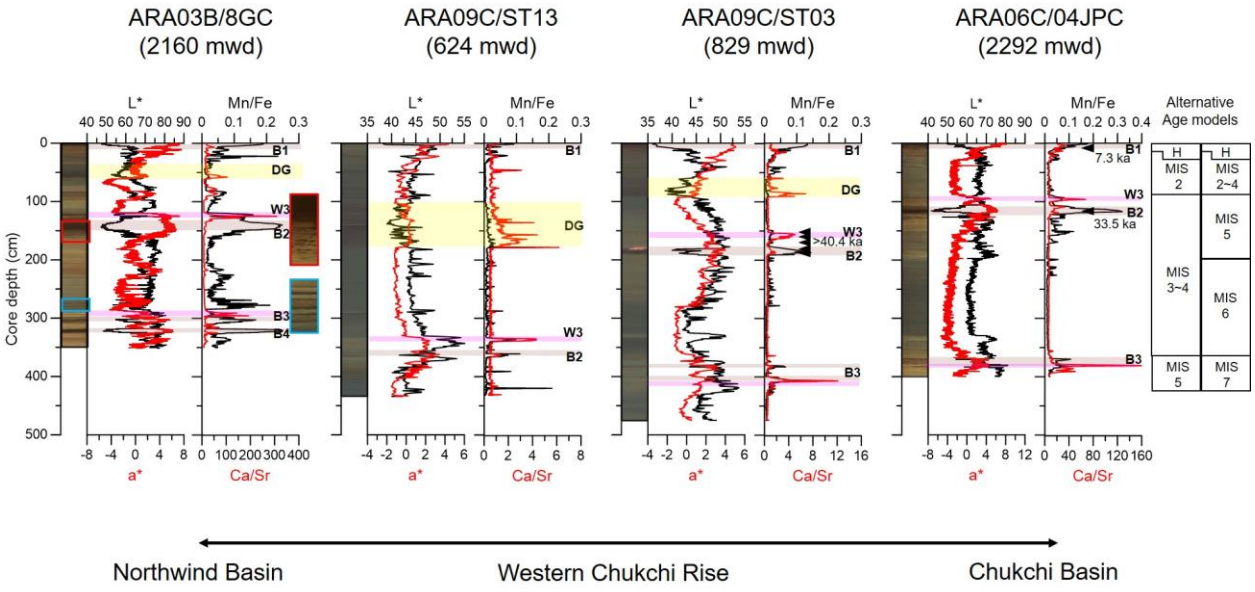

Figure 4. Lithostratigraphy of study cores based on core images, color indices (L*, a*), and XRF Mn/Fe and Ca/Sr ratios. See Fig. 1 for the core location. Light brown, pink, and yellow horizontal bars indicate the intervals of brown units B1-B3, pinkish-white layers with detrital carbonates (including layer W3), and dark gray interval (DG), respectively. Gray units G1-G2 are not highlighted. Red and blue boxes show zoomed-in images of the homogenous and laminated brownish intervals. Calibrated ^{14}C ages are shown for cores ST03 and 04JPC (see Table 2). Two alternative age models (MIS for Marine Isotope Stages; H for Holocene) are shown on the right; see text for more explanation.

4.2.2 Grain size

The brown units B1-B4 generally consist of mud to sandy mud, containing approximately 5-20% coarse particles larger than 63 μm. The overall content of clay and silt ranges from ~30% to 60% (Fig. 5). The gray units G1-G2 exhibit geographic variability in grain size. In cores 8GC, ST13, and ST03 from the Chukchi Borderland and Rise, G units are composed of silty to sandy mud and some coarse particles. In contrast, G units in core 04JPC from the Chukchi Basin are finer-grained without coarse particles. On the Chukchi Borderland, the G1 unit is characterized by increased silt and coarse particle content at the bottom of the DG unit. In the Chukchi Basin, the G1 unit of core 04JPC exhibits an up-core increase in the silt content while the clay content decreases upward. In core 8GC (Northwind Basin), the G2 unit shows an increase in the silt content in the lower part, followed by a decrease above ~220 cm of the core depth (Fig. 5). The up-core variations in clay and coarse particle contents are opposite to the silt content. In core ST03 (western Chukchi Rise), the silt content is relatively low in the lower part (328-375 cm). In the upper part, the silt content increases upward and decreases above 245 cm. The up-core variations in clay and coarse particle contents anti-correlate with the silt content. Similar characteristics are present in core 04JPC. Pinkish layers mainly consist of sandy mud. Their silt content is lower (~35-58%) than the DG unit (Fig. 5). The pink-white layer W3, identified above the B2 unit, gradually increases the clay content from the Northwind Basin to the Chukchi Basin. Another pinkish layer near the B3 unit shows no apparent geographic variation in grain size.

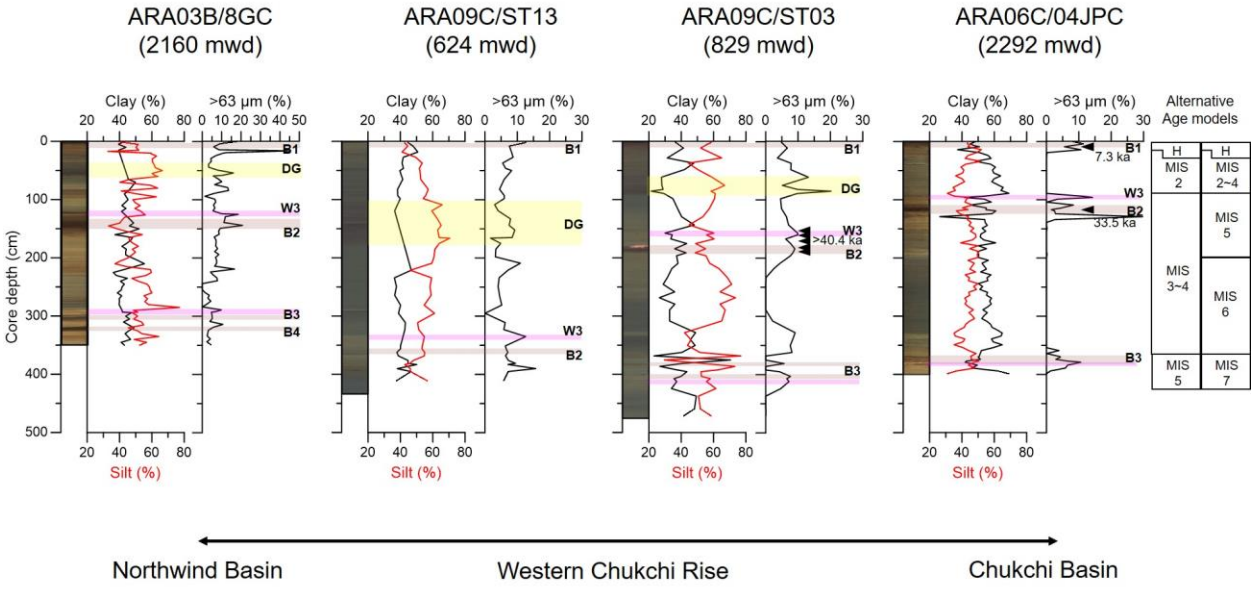

Figure 5. Down-core variation in major grain size fractions. Lithology and age interpretation as in Fig. 4.

4.2.3 Quartz, Plagioclase, and dolomite contents

The major minerals in the investigated sediment cores are quartz and plagioclase, which range from 16.4% to 25.2% and from 10.8% to 13.3% in average values, respectively (Fig. 6). Dolomite is relatively minor (1.4-5.0% on average), but increasing (up to ~32.6%) prominently in specific lithostratigraphies. Increases (up to ~40%) in quartz content are identified within and above the DG unit. In the upper part of the G1 unit, including the DG unit, variations in plagioclase are anti-correlated with those in quartz. Below the DG unit, the content of plagioclase is relatively high with small fluctuations similar to quartz variations. Dolomite increases slightly in the B units, while its abundance is very low in the G units. Pronounced dolomite peaks are identified in the DG unit and pinkish layers, corresponding to decreases in plagioclase. In all cores, the Q/F ratio generally co-varies with dolomite. In core 04JPC (Chukchi Basin), the Q/F ratio ranges from 0.2 to 0.9, with an average value of 0.4. In comparison, cores ST13 and ST03 (Chukchi Rise) have a higher Q/F ratio (>1). The spatial variation in the Q/F ratio in our cores is generally consistent with its increase from the East Siberian margin to the Alaska margin [*Darby et al.*, 2011; *Kobayashi et al.*, 2016; *Yamamoto et al.*, 2017; *Zou*, 2016].

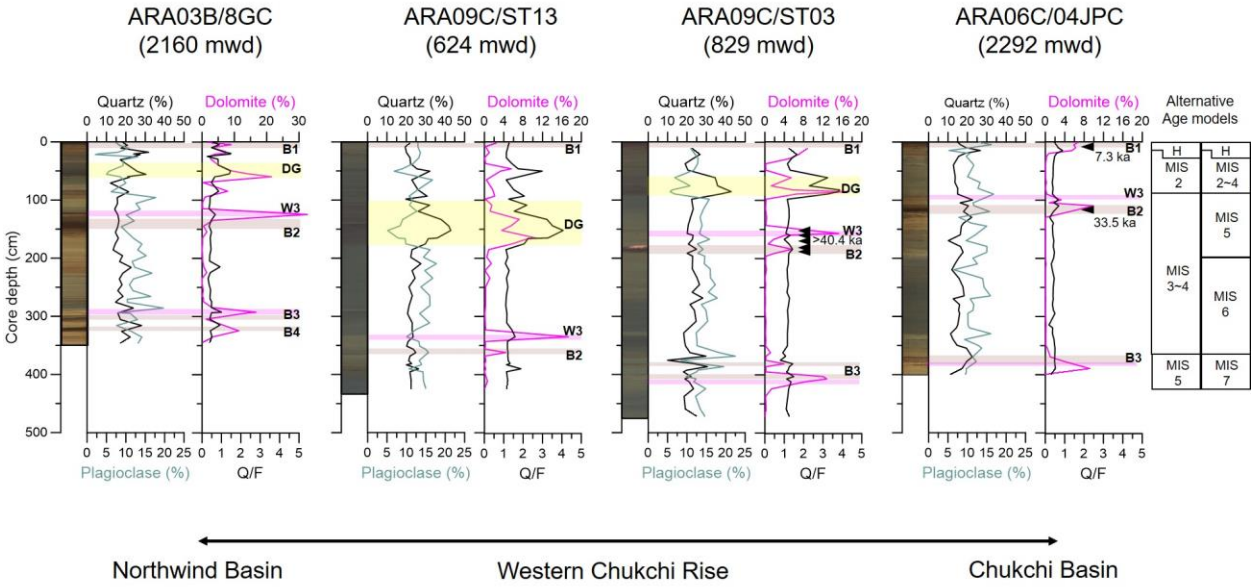

Figure 6. Down-core variation in bulk mineral composition (quartz, plagioclase/K-feldspar (Plg/KFS), dolomite, quartz/feldspar (Q/F)). Lithology and age interpretation as in Fig. 4.

4.2.4 AMS ^{14}C ages

In core 04JPC, the ^{14}C ages of 7.3 cal. ka and 33.5 ka were obtained at 5-6 cm in the B1 unit and 113-114 cm in the B2 unit, respectively (Fig. 4). In core ST03, three ^{14}C ages measured in intervals from 151 cm to 187 cm, including the W3 layer and B2 unit, are older than 40 ka (Fig. 4).

5 Discussion

5.1 Lithostratigraphic chronology

The chronology of the Arctic Ocean sediments is a matter of prolonged debate. Some studies propose chronostratigraphic constraints based primarily on the radiogenic isotope chronology [*Song et al.*, 2024 and references therein] or paleomagnetic inclination pattern [*Frederichs*, 1995; *Steuerwald et al.*, 1968]. Other authors focus on the cyclic lithostratigraphic alternation interpreted as a succession of glacial and interglacial/interstadial periods [e.g., *Jakobsson et al.*, 2000; *Polyak et al.*, 2009; *Stein et al.*, 2010]. While the chronostratigraphic methods arguably provide geochronological constraints for specific tie points, the litho/cyclostratigraphic approach offers a more comprehensive linkage to the climatic history. This linkage is especially evident in areas affected by glaciations, such as the Chukchi-East Siberian margin [*Joe et al.*, 2020; *Polyak et al.*, 2007; *Xiao et al.*, 2024]. However, establishing the age framework for glacial events requires calibration of the lithostratigraphy by independent age constraints, which is problematic for deposits older than the last deglaciation. While multiple ^{14}C ages have been generated for sediments underlying the last apparent glacial interval, such as in unit B2 (Fig. 4), these ages are uniformly older than ~35 ka and cannot be definitively interpreted. Considering these uncertainties, we do not define the absolute age model for the recovered stratigraphy but refer to the main lithostratigraphic units as the last and penultimate glacial/interglacial(interstadial) deposits with a discussion of the possible age range. This approach is adequate for coupling glacial dynamics imprinted in glacigenic bedforms with

depositional environments and provenance indicated by sediment cores, thus reconstructing the regional glacial history.

Lithostratigraphic units identified in cores under study based on lithological characteristics, including sediment color and structure, grain size, and Mn and Ca variations (Fig. 4), are correlative to the previously investigated sediment cores from the western Arctic Ocean [e.g., *Adler et al.*, 2009; *Joe et al.*, 2020; *Polyak et al.*, 2009; *Schreck et al.*, 2018; *Stein et al.*, 2010; *Zhang et al.*, 2019]. Dark brown units represent interglacial/major interstadial environments, consistent with ^{14}C ages from the uppermost interval B1 corresponding to the Holocene (Fig. 4). The previous brown unit B2 has been attributed in most studies to the MIS 3 interstadial (between ca. 25 and 60 ka). However, considering the uncertainty with the consistently old ^{14}C ages in this interval, we cannot exclude its older age, such as the last interglacial (ca. 115-130 ka), i.e., Eemian. Until independent chronostratigraphic tools resolve the age model, we refer to this unit as a penultimate interglacial/interstadial interval. Accordingly, the grayish glacial units G1 and G2 may correspond to MIS 2/4 and MIS 4/6, respectively (Fig. 5). The dark gray (DG) unit is consistently observed in sediment cores from the Chukchi Rise and Northwind Basin in the upper part of G1. A correlative interval in cores from the Chukchi margin characterized by abundant coal particles was constrained to the early part of the last deglaciation, around 12-15 ka [*Zhang et al.*, 2019]. Intervals with high/low-Mn interlamination, such as below the B2 unit, have also been attributed in cores off the Chukchi/East Siberian margin to deglacial processes [*Rujian Wang et al.*, 2013; *Xiao et al.*, 2024].

5.2 Stratigraphic constraints for glacigenic submarine landforms

In the seismic record from the western Chukchi Rise, the sub-seafloor reflector R2 correlates with the pinkish-white detrital carbonate layer W3 (Figs. 7A, B). This reflection pattern might be comparable to the East Siberian margin data, including the adjacent Arliss Plateau [Fig. 6 in *Joe et al.*, 2020]. However, in the Chukchi Rise records, the SSU 1 above R2 is characterized by a distinct stratification with moderate to strong amplitudes, differing from a transparent to slightly fuzzy SSU 1 signature on the eastern slope of the Arliss Plateau [*Joe et al.*, 2020]. This stratification is apparently related to the deposition of the DG unit localized on the Chukchi Rise and adjacent areas (Figs 7A, B). The next significant reflector, Rm, corresponds to the lower boundary of the outermost recessional moraine on the Chukchi Rise (Fig. 7A), marking the ice grounding event [*S Kim et al.*, 2021]. A stratigraphically short core ST13 does not recover sediments corresponding to Rm. However, in the deeper MSGL field, the reflector corresponding to Rm correlates with the sandy interval in the lower part of the G2 unit in core ST03 (Fig. 7B). This sandy sediment probably indicates that the deposition of the G2 unit is related to the formation of the outermost moraine on the western Chukchi Rise. Based on these seismostratigraphic constraints, SSU 1 and SSU 2, bound by the reflectors R1-R2 and R2-Rm, correspond to the last two glacial cycles affecting the Chukchi/East Siberian margin. The MSGL mapped at deeper water depths is buried or draped by well-stratified sediments with a more extended stratigraphy (Fig. 7B) and thus represents an older glaciation, consistent with the interpretation of *S Kim et al.* [2021].

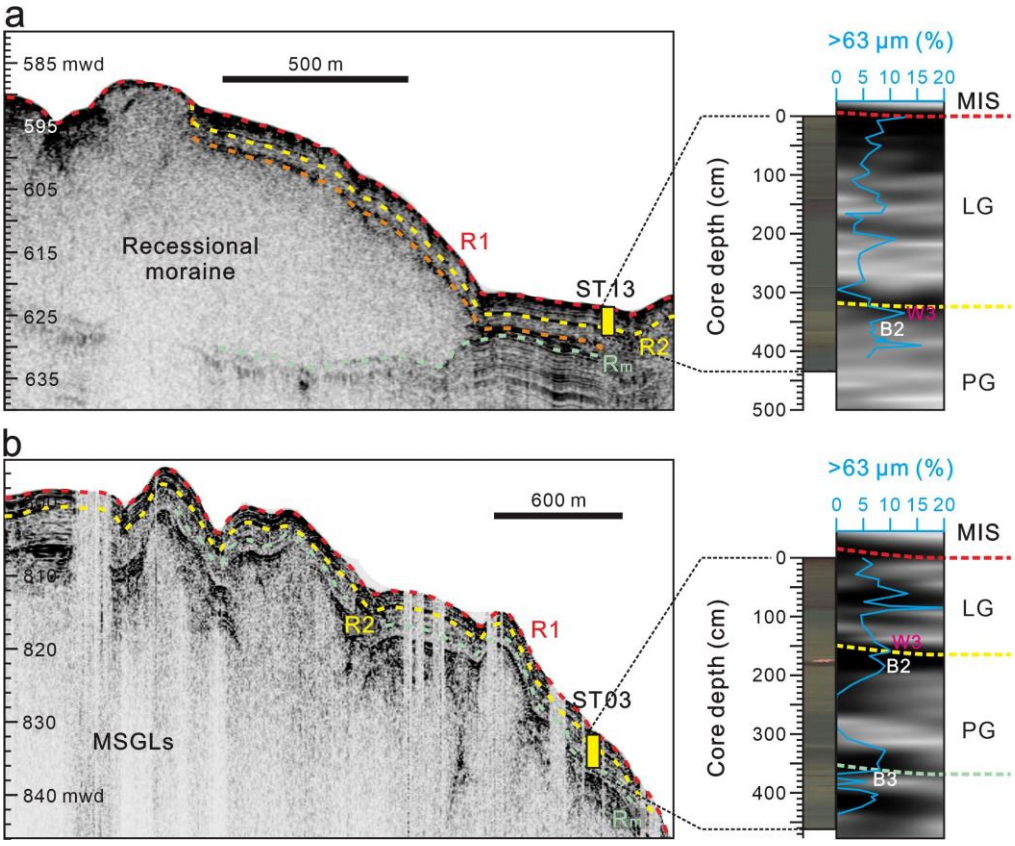

Figure 7. Core-seismic correlations on the western Chukchi Rise. (a) Subbottom profiling data (SBP) and core ST13 collected near a recessional moraine on the slope of the Chukchi Rise. (b) SBP and core ST13 record from deposits on top of MSGLs on the lower slope. See Figs. 2 and 3 for location and seismostratigraphic explanation, respectively. LG and PG – last glacial/deglacial and penultimate glacial/deglcial.

5.3 Sediment deposition and provenance

The elemental composition of sediments in the Arctic Ocean can provide initial clues to their origin. In particular, Ca peaks in the Arctic Ocean sediments generally correspond to the enhanced input of detrital carbonates, indicating primarily glacier-derived products of carbonate rocks from the Paleozoic platform in the Canadian Arctic Archipelago (CAA) [*Bazhenova et al.*, 2017; *Dong et al.*, 2017; *Polyak et al.*, 2009; *Stokes et al.*, 2005]. This affinity is supported by a good correspondence of the XRF Ca/Sr ratio (Fig. 4) and XRD dolomite peaks (Fig. 6). The prominent peaks in both proxies co-occur with the pinkish-white layers or lenses used as markers of iceberg discharge events from the western CAA area of the LIS [e.g., *Clark et al.*, 1980; *Polyak et al.*, 2009; *Stein et al.*, 2010]. These dolomite-rich intervals at the B3 unit, the W3 layer, the DG unit (the last deglaciation), and the bottom of the B1 unit (early Holocene) in the studied cores are consistent with the lithostratigraphy of other western Arctic Ocean records [*Dong et al.*, 2017; *Joe et al.*, 2020; *Schreck et al.*, 2018; *Xiao et al.*, 2024].

In addition to dolomite, other minerals can provide further insight into sediment provenance. The abundant presence of quartz is contributed by multiple Arctic sources, including much of the Siberian margin and parts of the Canadian Arctic [*Phillips and Grantz*, 2001]. High

values of quartz/feldspar (Q/F) ratio, such as in and above the DG unit (Fig. 6), have been associated with inputs to the Chukchi margin from Alaska and the Mackenzie River area [*Kobayashi et al.*, 2016; *Vogt*, 1997; *Zou*, 2016]. In comparison, the G1 and G2 units exhibit an increased plagioclase content (Fig. 6), more indicative of the Siberian margin [*Zhang et al.*, 2021; *Zou*, 2016].

Abundant coarse particles (>63 μm) are primarily associated with detrital carbonate layers (Fig. 5), consistent with their iceberg-rafted origin. However, the size of iceberg-rafted debris (IRD) depends on the type of deposits eroded by glaciers. While the LIS-eroded Paleozoic platform produces large amounts of coarse fragments [*Dong et al.*, 2017; *Dong et al.*, 2020; *England et al.*, 2009; *Polyak et al.*, 2009], this is not the case for unconsolidated clay-rich sediments of the Siberian shelves. As a result, glacial stratigraphic intervals with Siberian provenance in western Arctic cores are commonly fine-grained [*Dong et al.*, 2017; *Dong et al.*, 2020; *Rong Wang et al.*, 2021; *Xiao et al.*, 2024; *Ye et al.*, 2020]. This pattern is consistent with the clay-rich G units in core 04JPC from the Chukchi Basin (Fig. 5). Notably, the G2 unit in this and a nearby core 03M03 [*Rujian Wang et al.*, 2013] shows an expanded thickness. This sedimentary environment likely represents the deposition of glacial turbidites from the adjacent glaciated Chukchi/East Siberian margin to the Chukchi Basin as under- and/or overflows [*Dove et al.*, 2014; *Joe et al.*, 2020]. In comparison, the younger glacigenic unit G1 shows the highest thickness in core ST13 from the upper slope of the Chukchi Rise, possibly indicating its proximity to the marine-based ice sheet sourced from the Chukchi shelf.

5.4 Glaciation impacts on the Chukchi Borderland

Based on the developed provenance and litho/seismostratigraphic constraints combined with previously investigated seismic and sediment core records from adjacent areas [*Dong et al.*, 2017; *Dong et al.*, 2020; *Joe et al.*, 2020; *S Kim et al.*, 2021; *Polyak et al.*, 2007; *Rong Wang et al.*, 2021; *Xiao et al.*, 2024; *Zhang et al.*, 2019], we reconstruct major glacial events that affected the Chukchi margin during the Late Quaternary. The investigated sediment cores did not recover glacial deposits referred to as the deeper MSGL field on the lower slope of the Chukchi margin, based on geophysical data (Figs. 2, 3) [*S Kim et al.*, 2021]. In our records, the oldest iceberg discharge event in the studied cores may correspond to MIS 5.1, as suggested by several studies from the adjacent areas [*Dong et al.*, 2017; *Dong et al.*, 2020; *Joe et al.*, 2020; *Schreck et al.*, 2018; *Rong Wang et al.*, 2021]. However, studies using a different chronostratigraphic approach based on the uranium-series radiogenic isotopes infer an older age, possibly as old as MIS 7 [*Song et al.*, 2024].

The G2 unit is associated with the ice grounding event resulting in the deposition of the outermost recessional moraine on the western Chukchi Rise [*S Kim et al.*, 2021]. This glaciation corresponds to the last glacier erosion on the Arliss Plateau (core 16B-GC; Fig. 1) [*Joe et al.*, 2020]. The sediment composition of the G2 unit, characterized by high plagioclase content and the absence of dolomite/detrital carbonate (Fig. 6), indicates inputs from the East Siberian/Chukchi margin. A similar provenance has been shown for a correlative interval in cores from the adjacent areas, including the Northwind Ridge [*Dong et al.*, 2017; *Dong et al.*, 2020; *Rong Wang et al.*, 2021; *Ye et al.*, 2020]. This depositional pattern, with little to no input of CAA-sourced material, means that the Chukchi Rise and at least part of the Northwind Ridge were probably covered by the grounded ice from the East Siberian/Chukchi margin and/or its ice-shelf extension, which prevented the inflow of icebergs from the LIS (Fig. 8a). This

conclusion is consistent with evidence from seismostratigraphy and seafloor morphology indicating that the grounded ice mass spread from the Chukchi shelf onto the Chukchi Rise [*Dove et al.*, 2014; *S Kim et al.*, 2021]. Based on the distribution of glacigenic bedforms, such as morainic ridges and MSGL [*Dove et al.*, 2014; *Jakobsson et al.*, 2008; *S Kim et al.*, 2021; *Niessen et al.*, 2013], the ice grounding line extended to 600~700 mwd on the Chukchi Rise and nearly 950 mwd on the East Siberian margin (Fig. 8a). This configuration suggests that the major ice center was likely located on the East Siberian shelf. Nevertheless, a smaller Chukchi ice center (dome) was sufficiently large to control ice flow to the outer Chukchi margin, probably coalescing with ice from the East Siberian margin into one large ice sheet [*Jakobsson et al.*, 2014; *Lehmann and Jokat*, 2022]. Multiple directional bedforms, such as MSGL, indicate that a significant part of the Chukchi Borderland, especially the Northwind Ridge, was overridden by an ice shelf extending from the LIS at some point [*Dove et al.*, 2014; *Jakobsson et al.*, 2014; *Polyak et al.*, 2007]. MSGLs at the base of the Northwind Ridge with the LIS-sourced trajectory have been constrained to a pre-LGM, possibly MIS 4 glaciation [*Polyak et al.*, 2007], but older MIS 6 age cannot be excluded, as discussed above. This morphological configuration indicates potentially complex interactions of the LIS and Chukchi/East Siberian ice masses in this region, which is critical for comprehending the overall dynamics of Arctic marine-based ice sheets during the Late Quaternary. Further coupled geophysical and geological studies of the Chukchi Borderland are needed to understand these interactions.

The G1 unit, including the last deglacial deposits, differs considerably from the G2 unit. The characteristic feature of G1 is the abundance of detrital carbonate peaks, expressed by XRF Ca (Ca/Sr ratio) and dolomite content (Figs. 4, 6). In the upper part of the B2 unit, the deposition of the W3 layer is indicative of the LIS iceberg discharge event(s). This stratigraphic position could correspond to the onset of the Late Wisconsinian glaciation in the last MIS 3, soon after about 40 ka BP [*Dalton et al.*, 2019], or to MIS 4. Younger carbonate peaks are prominent in the DG unit (last deglaciation) and at the base of the B1 unit (Holocene), correlative with the post-LGM deglacial records from the Chukchi and East Siberian margins [*Schreck et al.*, 2018; *Xiao et al.*, 2024; *Ye et al.*, 2020; *Zhang et al.*, 2019]. This pattern can be explained by short-term deglacial surges of the CAA and Mackenzie lobes of the northwestern LIS, recorded in several higher-resolution sediment cores collected from the Chukchi-Alaskan margin [*Klotsko et al.*, 2019; *Zhang et al.*, 2019]. In the last deglaciation interval, the maxima in quartz and dolomite are interrupted by increases in plagioclase (Fig. 6). This composition indicates a discharge event from the Chukchi/East Siberian side. Previous studies show the impact of the Chukchi ice center during the LGM, based on geophysical data from the Chukchi Rise and southern Northwind Ridge, as well as sediment cores from the latter area and the adjacent Chukchi-Alaskan margin [*S Kim et al.*, 2021; *Polyak et al.*, 2007; *Zhang et al.*, 2019]. The LGM ice grounding on the southern Northwind Ridge was initially attributed to an ice mass extending from the LIS [*Polyak et al.*, 2007]. However, the MSGL pattern at the nearby margin of the Chukchi Rise indicates a more likely direction of the LGM ice movement from the Chukchi shelf [*S Kim et al.*, 2021]. The southern boundaries of this grounded ice mass have not been defined thus far due to intense seafloor erosion and sediment accumulation on the shallow shelf [*Dove et al.*, 2014]. Nevertheless, based on the available data, it can be estimated that the ice extent during the last glaciation was more restricted than during the previous glaciation of the Chukchi margin, with the LGM grounding line constrained to less than 450 mwd (Fig. 8b) [*S Kim et al.*, 2021; *Polyak et al.*, 2007].

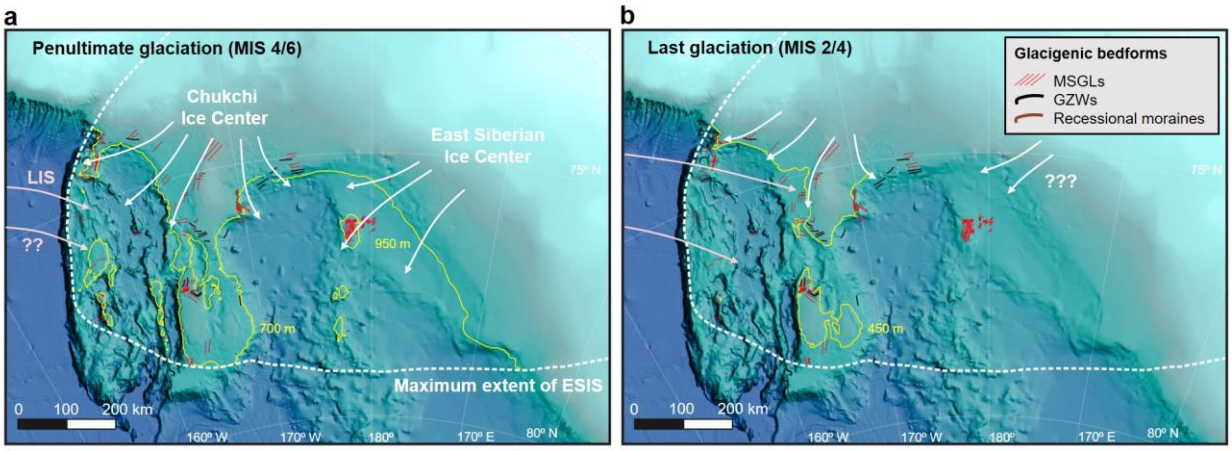

Figure 8. Inferred major glacial inputs to the Chukchi/East Siberian margin and ESIS grounding lines (yellow lines) during the last two glaciations. (a) The penultimate glaciation; note the grounding line change from ~950 mwd at the East Siberian margin to ~650 mwd at the Chukchi margin. (b) The last glaciation (grounding line shown for the Chukchi margin only). White and pinkish arrows for grounded ice movement and major iceberg events, respectively. The overall ESIS outline (white-dashed line) is adapted from *Lehmann and Jokat* [2022] and *Lehmann et al.* [2022].

Based on variations in bulk mineral composition of core 04JPC (Fig. 6), the deglacial LIS signature does not extend to the Chukchi Basin except for the lower part of the B1 unit, probably corresponding to the late deglacial stage ca. 9.5 ka BP [*Stokes et al.*, 2009]. This pattern, consistent with other cores west of the Chukchi Rise [*Schreck et al.*, 2018; *Zhang et al.*, 2019], could be related to a lingering ice shelf in this area, which blocked access to icebergs drifting from the LIS. Instead of the LIS-sourced material, an increased plagioclase content in the lower part of the G1 unit (Fig. 6) and a correlative clay mineral assemblage in core 03M03 [*Ye et al.*, 2020] indicate the predominance of Siberian inputs. However, it remains to be determined whether this composition is related to the East Siberian or Chukchi shelves. More seafloor data from the East Siberian margin are needed to verify the potential presence of the ESIS during the LGM.

6. Conclusions

To gain insight into the complex glacial history of the Chukchi/East Siberian Arctic margin, we investigated high-resolution swath bathymetry and subsurface seismostratigraphic records and sediment cores from the Chukchi Rise and the adjacent Chukchi and Northwind basins with a focus on the last two glaciations.

The penultimate glacial/deglacial interval has an estimated age range from MIS 6 to MIS 4/early MIS 3. For this period, the sediment records are predominantly characterized by Siberian–sourced material with high plagioclase content and rare or absent dolomite. This composition suggests that there were either minimal or no sediment inputs from icebergs originating from the Laurentide Ice Sheet. In comparison, peaks of iceberg-rafted debris (dolomite combined with high quartz content) from the Canadian Arctic Archipelago provenance were prominent above and below this interval. These variations in mineral composition indicate the extension of the East Siberian/Chukchi ice masses (marine-based glacier/ice shelf) to the

Chukchi Rise, which prevented iceberg transport from the LIS. By integrating seismostratigraphy with sediment core lithostratigraphy, we constrain the moraine formation at ~600-650 mwd on the western slope of the Chukchi Rise to this glaciation. Considering the ~950 mwd of the correlative glacial erosion on the Arliss Plateau, our results confirm that the ESIS extended to water depths of ~650 m on the Chukchi Rise and about 300 m deeper on the East Siberian margin. This distribution of the ESIS extent indicates that its major ice spreading center was likely located on the East Siberian margin, with a considerably large additional center on the Chukchi shelf.

In comparison, sediments of the last glaciation and deglaciation (MIS 2 to possibly MIS 4) have multiple peaks of dolomite and quartz, indicating prominent inputs of the LIS material. The upper part of this glacial unit in cores from the Chukchi Rise and the Northwind Basin contains a characteristic dark gray sediment. This interval likely represents early deglacial input from the Mackenzie area, as previously identified in multiple cores from the Chukchi margin [*Xiao et al.*, 2024; *Zhang et al.*, 2019]. An intermittent deglacial interval with the Siberian provenance indicates inputs from the Chukchi/East Siberian shelf areas. In the Chukchi Basin, the corresponding glacial to deglacial interval is mainly characterized by the Siberian provenance except for peaks of the LIS material at the onset of the last glacial unit and late deglaciation, which is consistent with clay mineral data in the correlative records. This Siberian signature indicates the potential presence of a grounded LGM ice at the East Siberian margin during MIS 2. However, further geophysical/geological investigations are needed to verify this glacial advance.

Acknowledgments

We thank the captain, crews, and KOPRI members who supported data collection during the ARAON arctic cruises. Dr. Hyo Jin Koo provided and prepared geophysical and mineralogical data. We also thank Drs. Jaesoo Lim and Gee Soo Kong at KIGAM helped with grain size analysis and XRF core scanning of the Chukchi Basin core, respectively.

Open Research

The processed SBP images and results of sediment core measurements used in this study are available at the Korea Polar Data Center (https://doi.org/10.22663/KOPRI-KPDC-00002442.1).

References

Adler, R. E., L. Polyak, J. D. Ortiz, D. S. Kaufman, J. E. Channell, C. Xuan, A. G. Grottoli, E. Sellén, and K. A. Crawford (2009), Sediment record from the western Arctic Ocean with an improved Late Quaternary age resolution: HOTRAX core HLY0503-8JPC, Mendeleev Ridge, *Global and Planetary Change*, *68*(1-2), 18-29.

Batchelor, C. L., M. Margold, M. Krapp, D. K. Murton, A. S. Dalton, P. L. Gibbard, C. R. Stokes, J. B. Murton, and A. Manica (2019), The configuration of Northern Hemisphere ice sheets through the Quaternary, *Nature Communications*, *10*(1), 3713, doi:10.1038/s41467-019-11601-2.

Bazhenova, E., N. Fagel, and R. Stein (2017), North American origin of "pink–white" layers at the Mendeleev Ridge (Arctic Ocean): New insights from lead and neodymium isotope composition of detrital sediment component, *Marine Geology*, *386*, 44-55.

Clark, D. L., R. R. Whitman, K. A. Morgan, and S. D. Mackey (1980), Stratigraphy and glacial-marine sediments of the Amerasian Basin, central Arctic Ocean.

Coulthard, R. D., M. F. Furze, A. J. Pieńkowski, F. C. Nixon, and J. H. England (2010), New marine ΔR values for Arctic Canada, *Quaternary Geochronology*, *5*(4), 419-434.
Dalton, A. S., S. A. Finkelstein, S. L. Forman, P. J. Barnett, T. Pico, and J. X. Mitrovica (2019), Was the Laurentide Ice Sheet significantly reduced during marine isotope stage 3?, *Geology*, *47*(2), 111-114.
Dalton, A. S., C. R. Stokes, and C. L. Batchelor (2022), Evolution of the Laurentide and Innuitian ice sheets prior to the Last Glacial Maximum (115 ka to 25 ka), *Earth-Science Reviews*, *224*, 103875.
Darby, D. A., W. B. Myers, M. Jakobsson, and I. Rigor (2011), Modern dirty sea ice characteristics and sources: The role of anchor ice, *Journal of Geophysical Research: Oceans*, *116*(C9).
Dong, L., Y. Liu, X. Shi, L. Polyak, Y. Huang, X. Fang, J. Liu, J. Zou, K. Wang, and F. Sun (2017), Sedimentary record from the Canada Basin, Arctic Ocean: implications for late to middle Pleistocene glacial history, *Climate of the Past*, *13*(5), 511-531.
Dong, L., L. Polyak, Y. Liu, X. Shi, J. Zhang, and Y. Huang (2020), Isotopic fingerprints of ice-rafted debris offer new constraints on Middle to Late Quaternary Arctic circulation and glacial history, *Geochemistry, Geophysics, Geosystems*, *21*(8), e2020GC009019.
Dove, D., L. Polyak, and B. Coakley (2014), Widespread, multi-source glacial erosion on the Chukchi margin, Arctic Ocean, *Quaternary Science Reviews*, *92*, 112-122.
England, J. H., M. F. Furze, and J. P. Doupe (2009), Revision of the NW Laurentide Ice Sheet: implications for paleoclimate, the northeast extremity of Beringia, and Arctic Ocean sedimentation, *Quaternary Science Reviews*, *28*(17-18), 1573-1596.
Fagel, N., C. Not, J. Gueibe, N. Mattielli, and E. Bazhenova (2014), Late Quaternary evolution of sediment provenances in the Central Arctic Ocean: mineral assemblage, trace element composition and Nd and Pb isotope fingerprints of detrital fraction from the Northern Mendeleev Ridge, *Quaternary Science Reviews*, *92*, 140-154.
Ferrat, M., D. J. Weiss, B. Spiro, and D. Large (2012), The inorganic geochemistry of a peat deposit on the eastern Qinghai-Tibetan Plateau and insights into changing atmospheric circulation in central Asia during the Holocene, *Geochimica et Cosmochimica Acta*, *91*, 7-31.
Frederichs, T. (1995), Regional and temporal variations of rock magnetic parameters in Arctic marine sediments, *Berichte zur Polarforschung*, *164*, 1-212.
Gasson, E. G., R. M. DeConto, D. Pollard, and C. D. Clark (2018), Numerical simulations of a kilometre-thick Arctic ice shelf consistent with ice grounding observations, *Nature communications*, *9*(1), 1-9.
Hanslik, D., M. Jakobsson, J. Backman, S. Björck, E. Sellén, M. O'Regan, E. Fornaciari, and G. Skog (2010), Quaternary Arctic Ocean sea ice variations and radiocarbon reservoir age corrections, *Quaternary Science Reviews*, *29*(25-26), 3430-3441.
Heaton, T. J., P. Köhler, M. Butzin, E. Bard, R. W. Reimer, W. E. Austin, C. B. Ramsey, P. M. Grootes, K. A. Hughen, and B. Kromer (2020), Marine20—the marine radiocarbon age calibration curve (0–55,000 cal BP), *Radiocarbon*, *62*(4), 779-820.
Hodell, D. A., J. E. Channell, J. H. Curtis, O. E. Romero, and U. Röhl (2008), Onset of "Hudson Strait" Heinrich events in the eastern North Atlantic at the end of the middle Pleistocene transition (~ 640 ka)?, *Paleoceanography*, *23*(4).
Hu, A., G. A. Meehl, B. L. Otto-Bliesner, C. Waelbroeck, W. Han, M.-F. Loutre, K. Lambeck, J. X. Mitrovica, and N. Rosenbloom (2010), Influence of Bering Strait flow and North Atlantic circulation on glacial sea-level changes, *Nature Geoscience*, *3*(2), 118-121.
Jakobsson, M., K. Andreassen, L. R. Bjarnadóttir, D. Dove, J. A. Dowdeswell, J. H. England, S. Funder, K. Hogan, Ó. Ingólfsson, and A. Jennings (2014), Arctic Ocean glacial history, *Quaternary Science Reviews*, *92*, 40-67.
Jakobsson, M., R. Løvlie, H. Al-Hanbali, E. Arnold, J. Backman, and M. Mörth (2000), Manganese and color cycles in Arctic Ocean sediments constrain Pleistocene chronology, *Geology*, *28*(1), 23-26.
Jakobsson, M., L. A. Mayer, C. Bringensparr, C. F. Castro, R. Mohammad, P. Johnson, T. Ketter, D. Accettella, D. Amblas, and L. An (2020), The international bathymetric chart of the Arctic Ocean version 4.0, *Scientific data*, *7*(1), 1-14.
Jakobsson, M., J. Nilsson, L. Anderson, J. Backman, G. Björk, T. M. Cronin, N. Kirchner, A. Koshurnikov, L. Mayer, and R. Noormets (2016), Evidence for an ice shelf covering the central Arctic Ocean during the penultimate glaciation, *Nature Communications*, *7*(1), 1-10.
Jakobsson, M., L. Polyak, M. Edwards, J. Kleman, and B. Coakley (2008), Glacial geomorphology of the central Arctic Ocean: the Chukchi Borderland and the Lomonosov Ridge, *Earth Surface Processes and Landforms: The Journal of the British Geomorphological Research Group*, *33*(4), 526-545.

650 Jang, K., Y. Han, Y. Huh, S.-I. Nam, R. Stein, A. Mackensen, and J. Matthiessen (2013), Glacial freshwater
651 discharge events recorded by authigenic neodymium isotopes in sediments from the Mendeleev Ridge, western
652 Arctic Ocean, *Earth and Planetary Science Letters*, *369*, 148-157.
653 Jang, K., K. S. Woo, J.-K. Kim, and S.-I. Nam (2023), Arctic deep-water anoxia and its potential role for ocean
654 carbon sink during glacial periods, *Communications Earth & Environment*, *4*(1), 45.
655 Joe, Y. J., L. Polyak, M. Schreck, F. Niessen, S. H. Yoon, G. S. Kong, and S.-I. Nam (2020), Late Quaternary
656 depositional and glacial history of the Arliss Plateau off the East Siberian margin in the western Arctic Ocean,
657 *Quaternary Science Reviews*, *228*, 106099.
658 Kim, S., L. Polyak, Y. J. Joe, F. Niessen, H. J. Kim, Y. Choi, S. G. Kang, J. K. Hong, S. I. Nam, and Y. K. Jin
659 (2021), Seismostratigraphic and geomorphic evidence for the glacial history of the northwestern Chukchi margin,
660 Arctic Ocean, *Journal of Geophysical Research: Earth Surface*, *126*(4), e2020JF006030.
661 Kim, Y.-G., S. Kim, D.-H. Lee, Y. M. Lee, H. J. Kim, S.-G. Kang, and Y. K. Jin (2020), Occurrence of active gas
662 hydrate mounds in the southwestern slope of the Chukchi Plateau, Arctic Ocean, *Episodes Journal of International*
663 *Geoscience*, *43*(2), 811-823.
664 Klotsko, S., N. Driscoll, and L. Keigwin (2019), Multiple meltwater discharge and ice rafting events recorded in the
665 deglacial sediments along the Beaufort Margin, Arctic Ocean, *Quaternary Science Reviews*, *203*, 185-208.
666 Kobayashi, D., M. Yamamoto, T. Irino, S.-I. Nam, Y.-H. Park, N. Harada, K. Nagashima, K. Chikita, and S.-I.
667 Saitoh (2016), Distribution of detrital minerals and sediment color in western Arctic Ocean and northern Bering Sea
668 sediments: Changes in the provenance of western Arctic Ocean sediments since the last glacial period, *Polar*
669 *Science*, *10*(4), 519-531.
670 Koo, H.-J., Y.-K. Jin, and H.-G. Cho (2021), Change in Sediment Provenance on the Inner Slope of the Chukchi
671 Rise and Their Paleoenvironmental Implications, *Applied Sciences*, *11*(14), 6491.
672 Koo, H. J., J. K. Jang, D. H. Lee, and H. G. Cho (2022), Authigenic Gypsum Precipitation in the ARAON Mounds,
673 East Siberian Sea, *Minerals*, *12*(8), 983.
674 Lehmann, C., and W. Jokat (2022), Seismic constraints for ice sheets along the northern margin of Beringia, *Global*
675 *and Planetary Change*, *215*, 103885.
676 Lehmann, C., W. Jokat, and B. Coakley (2022), Glacial sediments on the outer Chukchi Shelf and Chukchi
677 Borderland in seismic reflection data, *Marine Geophysical Research*, *43*(3), 1-16.
678 Niessen, F., et al. (2013), Repeated Pleistocene glaciation of the East Siberian continental margin, *Nature*
679 *Geoscience*, *6*(10), 842-846.
680 O'Regan, M., J. Backman, N. Barrientos, T. M. Cronin, L. Gemery, N. Kirchner, L. A. Mayer, J. Nilsson, R.
681 Noormets, and C. Pearce (2017), The De Long Trough: a newly discovered glacial trough on the East Siberian
682 continental margin, *Climate of the Past*, *13*(9), 1269-1284.
683 Peltier, W. (2007), Rapid climate change and Arctic Ocean freshening, *Geology*, *35*(12), 1147-1148.
684 Phillips, R., and A. Grantz (2001), Regional variations in provenance and abundance of ice-rafted clasts in Arctic
685 Ocean sediments: implications for the configuration of late Quaternary oceanic and atmospheric circulation in the
686 Arctic, *Marine Geology*, *172*(1-2), 91-115.
687 Polyak, L., J. Bischof, J. D. Ortiz, D. A. Darby, J. E. Channell, C. Xuan, D. S. Kaufman, R. Løvlie, D. A. Schneider,
688 and D. D. Eberl (2009), Late Quaternary stratigraphy and sedimentation patterns in the western Arctic Ocean,
689 *Global and Planetary Change*, *68*(1-2), 5-17.
690 Polyak, L., D. A. Darby, J. F. Bischof, and M. Jakobsson (2007), Stratigraphic constraints on late Pleistocene glacial
691 erosion and deglaciation of the Chukchi margin, Arctic Ocean, *Quaternary Research*, *67*(2), 234-245.
692 Polyak, L., M. H. Edwards, B. J. Coakley, and M. Jakobsson (2001), Ice shelves in the Pleistocene Arctic Ocean
693 inferred from glaciogenic deep-sea bedforms, *Nature*, *410*(6827), 453-457.
694 Schreck, M., S.-I. Nam, L. Polyak, C. Vogt, G.-S. Kong, R. Stein, J. Matthiessen, and F. Niessen (2018), Improved
695 Pleistocene sediment stratigraphy and paleoenvironmental implications for the western Arctic Ocean off the East
696 Siberian and Chukchi margins, *arktos*, *4*(1), 1-20.
697 Song, T., C. Hillaire-Marcel, A. de Vernal, and Y. Liu (2024), A resilient ice cover over the southernmost
698 Mendeleev Ridge during the late Quaternary, *Boreas*, *53*(1), 106-123.
699 Stein, R., J. Matthiessen, F. Niessen, A. Krylov, S.-i. Nam, and E. Bazhenova (2010), Towards a better (litho-)
700 stratigraphy and reconstruction of Quaternary paleoenvironment in the Amerasian Basin (Arctic Ocean),
701 *Polarforschung*, *79*(2), 97-121.
702 Steuerwald, B., D. Clark, and J. Andrew (1968), Magnetic stratigraphy and faunal patterns in Arctic Ocean
703 sediments, *Earth and Planetary Science Letters*, *5*, 79-85.

Stokes, C. R., C. D. Clark, D. A. Darby, and D. A. Hodgson (2005), Late Pleistocene ice export events into the Arctic ocean from the M'Clure strait ice stream, Canadian Arctic Archipelago, *Global and Planetary Change*, *49*(3-4), 139-162.

Stokes, C. R., C. D. Clark, and R. Storrar (2009), Major changes in ice stream dynamics during deglaciation of the north-western margin of the Laurentide Ice Sheet, *Quaternary Science Reviews*, *28*(7-8), 721-738.

Streuff, K. T., C. Ó Cofaigh, and P. Wintersteller (2021), A GIS Database of Submarine Glacial Landforms and Sediments on Arctic Continental Shelves, edited, PANGAEA, doi:10.1594/PANGAEA.937782.

Svendsen, J. I., H. Alexanderson, V. I. Astakhov, I. Demidov, J. A. Dowdeswell, S. Funder, V. Gataullin, M. Henriksen, C. Hjort, and M. Houmark-Nielsen (2004), Late Quaternary ice sheet history of northern Eurasia, *Quaternary Science Reviews*, *23*(11-13), 1229-1271.

Viscosi-Shirley, C., K. Mammone, N. Pisias, and J. Dymond (2003), Clay mineralogy and multi-element chemistry of surface sediments on the Siberian-Arctic shelf: implications for sediment provenance and grain size sorting, *Continental Shelf Research*, *23*(11-13), 1175-1200.

Vogt, C. (1997), *Regional and temporal variations of mineral assemblages in Arctic Ocean sediments as climatic indicator during glacial/interglacial changes*, Alfred-Wegener-Institut für Polar-und Meeresforschung.

Vogt, C. (2009), Data report: semiquantitative determination of detrital input to ACEX sites based on bulk sample X-ray diffraction data, paper presented at Proc. IODP| Volume.

Vogt, C., J. Lauterjung, and R. X. Fischer (2002), Investigation of the Clay Fraction (< 2 μm) of the Clay Minerals Society Reference Clays, *Clays and Clay Minerals*, *50*(3), 388-400.

Wang, R., L. Polyak, W. Zhang, X. Yu, L. Ye, L. Dong, Y. Liu, W. Wang, and B. Diekmann (2021), Glacial-interglacial sedimentation and paleocirculation at the Northwind Ridge, western Arctic Ocean, *Quaternary Science Reviews*, *258*, 106882.

Wang, R., W. Xiao, C. März, and Q. Li (2013), Late Quaternary paleoenvironmental changes revealed by multi-proxy records from the Chukchi Abyssal Plain, western Arctic Ocean, *Global and Planetary Change*, *108*, 100-118.

Xiao, W., L. Polyak, R. Wang, L. Löwemark, J. Mei, D. You, W. Wang, L. Wu, and X. Jin (2020), Middle to Late Pleistocene Arctic paleoceanographic changes based on sedimentary records from Mendeleev Ridge and Makarov Basin, *Quaternary Science Reviews*, *228*, 106105.

Xiao, W., L. Polyak, R. Wang, C. Not, L. Dong, Y. Liu, T. Ma, and T. Zhang (2021), A sedimentary record from the Makarov Basin, Arctic Ocean, reveals changing middle to Late Pleistocene glaciation patterns, *Quaternary Science Reviews*, *270*, 107176.

Xiao, W., L. Polyak, T. Zhang, R. Wang, X. Duan, Y. Tu, Y. Hu, and Y. Pan (2024), Depositional and circulation changes at the Chukchi margin, Arctic Ocean, during the last two glacial cycles, *Global and Planetary Change*, 104366.

Yamamoto, M., S.-I. Nam, L. Polyak, D. Kobayashi, K. Suzuki, T. Irino, and K. Shimada (2017), Holocene dynamics in the Bering Strait inflow to the Arctic and the Beaufort Gyre circulation based on sedimentary records from the Chukchi Sea, *Climate of the Past*, *13*(9), 1111-1127.

Ye, L., W. Zhang, R. Wang, X. Yu, and L. Jin (2020), Ice events along the East Siberian continental margin during the last two glaciations: Evidence from clay minerals, *Marine Geology*, *428*, 106289.

Zhang, T., R. Wang, L. Polyak, and W. Xiao (2019), Enhanced deposition of coal fragments at the Chukchi margin, western Arctic Ocean: Implications for deglacial drainage history from the Laurentide Ice Sheet, *Quaternary Science Reviews*, *218*, 281-292.

Zhang, T., R. Wang, W. Xiao, L. Polyak, A. Astakhov, L. Dong, C. Wang, Y. Liu, and X. Shi (2021), Characteristics of terrigenous components of Amerasian Arctic Ocean surface sediments: Implications for reconstructing provenance and transport modes, *Marine Geology*, *437*, 106497.

Zhao, S., Y. Liu, L. Dong, X. Shi, L. Polyak, X. Zou, W. Wang, and D. Wu (2022), Sedimentary record of glacial impacts and melt water discharge off the East Siberian Continental Margin, Arctic Ocean, *Journal of Geophysical Research: Oceans*, *127*(1), e2021JC017650.

Zou, H. (2016), An X-ray diffraction approach: bulk mineral assemblages as provenance indicator of sediments from the Arctic Ocean, Universität Bremen.